Design, Development, and Demonstration of a 1kW/10kWh Vanadium Redox Flow Battery System Minimizing Shunt Current Losses

Harun Khan[$], M. Raja[$], N.V.Sarma[#]. M. Nagarajan[#], J. Ramesh[#], G.A. Pathanjali[#] , Damaraju Parvatalu[f], Saroj Chaudhary[f] and R. Kothandaraman[$*]

[$]Clean Energy Lab, Department of chemistry, Indian institute of technology madras, Chennai 600036, Tamil Nadu, India

[#]High Energy Batteries (India) Limited, Mathur-622515, Tamil Nadu, India

[f]ONGC Energy Trust Centre, IEOT Complex, Phase-II, Panvel, Raigad 410221

*Corresponding author's e-mail: rkraman@iitm.ac.in

Abstract: Vanadium redox flow battery (VRFB) is one of the most explored technologies for large-scale energy storage applications. However, the shunt current loss is one of the main factors that affect the performance of the VRFB while stacking, which will shorten the cycle life and decrease the energy efficiency of this system. This article deals with the strategic development and demonstration of a 1kW/10kWh VRFB stack with an electrode area of 600 cm^2. Non-conducting polymeric flow frames (PFF) emulated bipolar and monopolar graphite plates with serpentine flow field were employed to build 24 cells VRFB stack devoid of shunt current loss. Besides, H_3PO_4 is explored as an additive to the vanadium electrolyte, which resulted in nearly a 15 % improvement in capacity retention compared to the neat vanadium electrolyte in sulfuric acid.

Keywords: Vanadium redox flow battery, 1kW/10kWh stack, energy storage, shunt current, Polarization

1. **Introduction**

Transition to the ultimate clean and green renewable energy sources from the highly polluting fossil fuels-based conventional energy sources demands a self-sustaining energy storage system. However, since renewable energy is highly seasonal and intermittent, its effective utilization is feasible only if an energy storage system is introduced between the grid and the renewable energy production system to buffer the excess energy available[1–3]. The extra energy produced will be stored in an energy storage system (ESS) and used in a planned manner as per the demand. This way, the intermittency issues associated with the energy production system can be handled [4–7]. Redox flow batteries (RFBs) are known ESS for load levelling and an emergency power supply system. Interestingly, compared to conventional batteries, RFBs have the distinct advantage of decoupled power and energy, high efficiency, deep discharge capability, and enhanced safety.

Among the various RFB technologies [8–11], vanadium redox flow batteries (VRFB) were extensively studied and tested in fields up to MW size [12–15]. VRFB has the advantage of operating with redox couples made of a single element, vanadium. The redox couples are V^{2+}/ V^{3+} and VO^{2+}/ VO_2^+ at negative and positive electrolytes. Therefore, even if vanadium ions crossover, the VRFB can be restored to its original condition by electrolysis method[16, 17].

Generally, stacks of rating 1 kW to 5kW are used to build MW scale commercial ESS[18,19]. The capacity and energy stored depend on the amount of the electrolyte and concentration of vanadium species; therefore, energy can be scaled up by increasing the size of tanks and the concentration of redox species hooked up with the stack[20]. However, while scaling up from a single-cell to a multi-cell stack, one of the main challenges is the shunt current loss as a result of using highly conducting electrolytes. Therefore, having a common channel for feeding all the electrode plates in the stack

generally leads to ions skipping and, inturn, shunt current loss[12, 21]. This effect will bring down the overall power of the system. Travo *et al.* suggested that the longer and thinner flow paths in the trade-off between shunt current and hydraulic losses, in the limit that flow channels do not risk being clogged[20]. A bigger-sized cell is preferred over stacking smaller-sized multiple cells to counter the shunt current loss. An experimental demonstration of a 10 kW VRFB stack by Park *et al.,* using 31 cells of 2714 cm^2 active area (without any flow channel grooves), reported energy efficiencies (EE) of 76 and 70 % for current densities of 60 and 90 mA cm^{-2} respectively[22].

Several stack studies have been reported with the cell area of 600 to 1800 cm^2 operated between 70 and 90 mA cm^{-2} current densities. In contrast, single-cell studies were reported at much higher current densities (40 to 400 mA cm^{-2}) with an EE of 80 to 90 % [23–27]. Most single-cell studies have been conducted on a small active area, typically 2 to 25 cm^2 at higher flow rates of 2 to 4 ml $min^{-1}cm^{-2}$. Generally, larger area cells, due to the high current, suffers from high ohmic over-potential, leading to lower EE. This calls for optimization of the area of the cell and the number of cells that make the stack. To counter the shunt current losses, as part of this work, we have developed a 1kW/10kWh VRFB stack with the modified manifold design, wherein polymeric flow frame (PFF) handles the flow perpendicular to the stack supplying electrolyte to the cells in the stack. As PFF is electrically non-conductive, the ions in the solution are not under the influence of an electric field until they enter the active area of the cell.

2. Experimental

2.1. Materials and methods

Vanadyl sulphate salt ($VOSO_4.xH_2O$, Trifin Industries, India) extra pure, sulfuric acid (H_2SO_4, assay 97 %, Renkem, India), graphite felt (GF) electrodes (Nickunz Eximp Entp Pvt Ltd, India), proton exchange membrane (Nafion®-117, Ion Power, USA), and graphite plates (Universal Graphite, New Delhi) are used for fabricating the single cells and multi-cell stacks. Mono-polar and bipolar plates were manufactured by machining the graphite plates and the PFFs. Thermally activated graphite felts (GF ~ 90 % porous) were used as electrode material. Nafion®-117 membrane is used as a separator as well as a proton conducting medium between the electrodes. Membranes are pre-treated by heating in 3 % *v/v* H_2O_2 followed by heating in 0.5 M H_2SO_4 at 80 °C for 30 min and stored under conductivity water prior to the experiments[28]. Copper current collectors, aluminium end support plates, polymeric spacers, and outlet nozzles (PVC) were used to assemble the 1 kW VRFB stack. PVC piping connections are used between the stack, pumps (Mackbow, India), and electrolyte tanks for the flow of anolyte and catholyte. For the electrolyte preparation, the required amount of $VOSO_4$ salt is dissolved in 3M sulfuric acid to make a 1.6 M vanadium electrolyte. 0.05 M phosphoric acid is added to the electrolyte as an additive to improve the capacity of the vanadium electrolyte.

The coulombic efficiency (CE), EE, and voltage efficiency (VE) are calculated, as per equations 1, 2 and 3, respectively.

$$CE = \frac{\int I_d\, dt}{\int I_c\, dt} \text{X } 100\ \% \qquad (1)$$

$$EE = \frac{\int V_d I_d\, dt}{\int V_c I_c\, dt} \text{X } 100\ \% \qquad (2)$$

$$VE = \frac{EE}{CE} \text{X } 100\ \% \qquad (3)$$

Where, I_d and I_c are discharge and charge currents, respectively. V_d and V_c are the discharge and charge voltages, respectively.

2.2. 1 kW/10 kWh VRFB stack assembly

1 kW VRFB stack is built using graphite plates with an active area of 600 cm^2. Fig. 1 shows the components of the bipolar plate for stack assembly. Fig 1(a) depicts the PFF front view and Fig 1(b) shows the side view of the graphite bipolar plate. The serpentine flow field is grooved on both sides of the graphite plate. The flow field comprises 5 passes of 6 serpentine U bends with a land and channel width of 1.5 and 1.2 mm, respectively. The graphite bipolar plate fitted inside the two PFFs with the provision

for an inlet and outlet for the electrolyte flow. The assembled bipolar plate with the 4 mm thick PVC spacer is shown in Fig 1(c). GF electrodes are placed inside the spacer. Two mono-polar plates and 23 bipolar plates are used in the stack of 24 cells. Two PVC nozzles with inner and outer diameters of 1.6 cm and 1.8 cm are fitted on both sides of the end plates as inlet and outlet for the electrolyte to flow.

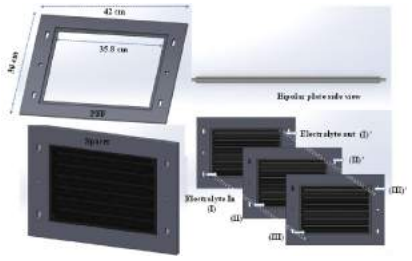


Fig. 1. Components of bipolar plates (a) PFF (b) side view of the bipolar plate assembly (c) assembled bipolar plate with PVC spacer and (d) flow direction of electrolyte from one plate to other

The assembled 24-cell stack photograph is shown in Fig. 2, wherein aluminium (blue in colour) end support plates are used for uniform compression. The membrane is flanked between the two graphite felts of each cell to obtain membrane electrode assembly (MEA). GF electrodes are accommodated in the spacer and a 1 mm thick rubber gasket is placed during the stack assembly. The gasket helps in mitigating any electrolyte leakage during the operation of VRFB. 1.6 M of V^{3+}(anolyte) solution is prepared from 1.6 M VO^{2+} in 3M H_2SO_4 solution electrochemically[29]. Freshly prepared 1.6 M VO^{2+} in 3M H_2SO_4 solution is used as catholyte. The flow rate of anolyte and catholyte is fixed at 15 lpm for 24 cells stack. Fig. 3 shows the schematic arrangement of the 1 kW/10 kWh VRFB stack assembly with pipe connections/tubing, pumps, electrolyte solutions, solar PV panels, and an inverter.

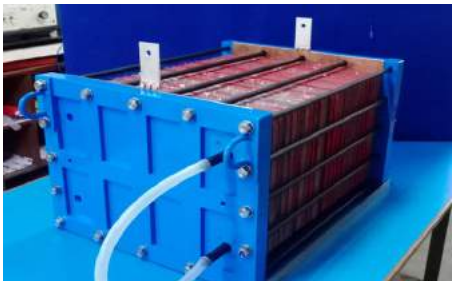


Fig. 2. Photograph of 24-cell VRFB stack.

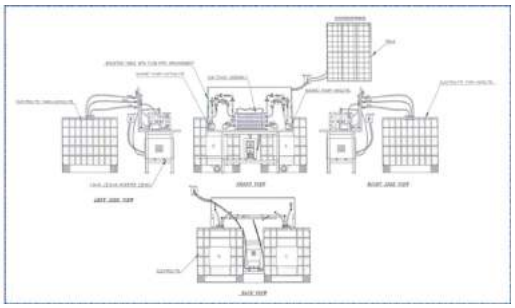
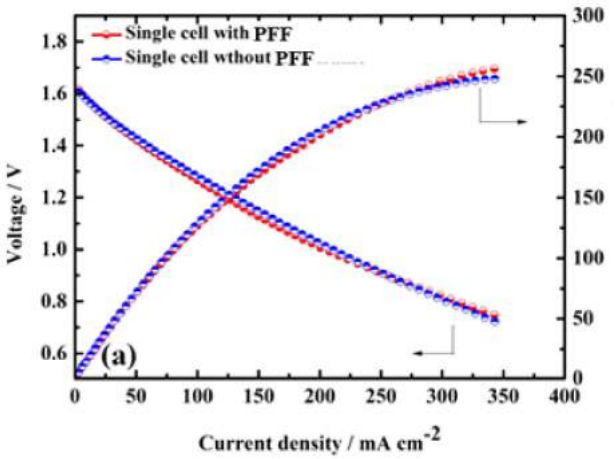


Fig. 3. Schematic arrangement drawing for 1 kW/10 kWh VRFB stack assembly

3. Results and discussion

3.1 Effect of PFF on the performance

It is challenging to measure the shunt current within the VRFB stack because of the difficulty and complexity of installing the current sensor or shunt coil in the manifold and flow channels. The non-uniform distribution of the electric current due to shunt current can lead to variation in voltage across the cells of the stack. As PFF is electrically non-conducting, the ions in the solution are not under the influence of an electric field at the inlet and outlet of the cell until they enter the bipolar plate region embedded in the PFF frame. Compared to having an entire plate out of graphite, the developed design gives a longer path for the solution, thereby mitigating the shunt current. The polarization measurements were carried out with and without PFF to understand the effect of PFF on reducing shunt current losses.



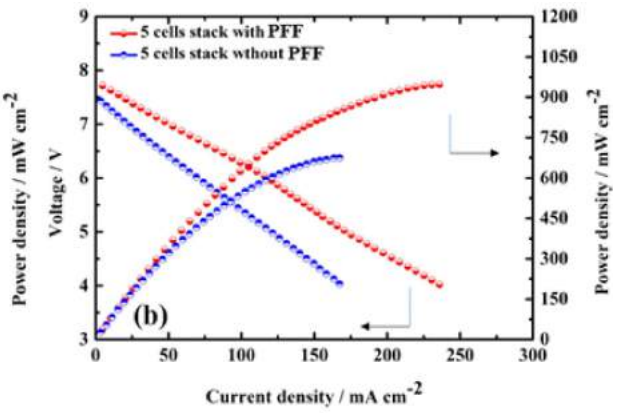
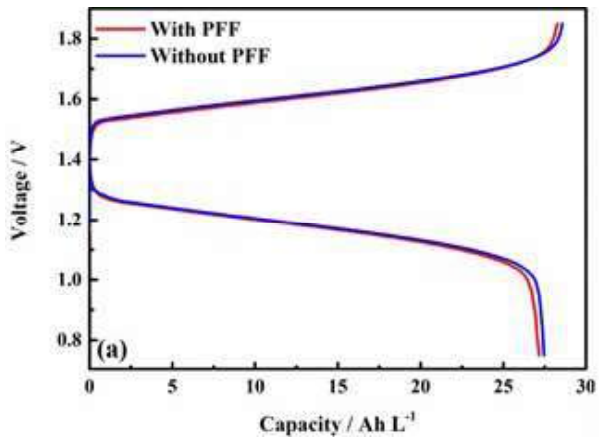


Fig. 4 Polarization (I-V) comparison plots of VRFB (a) single-cell and (b) 5-cell stack with and without PFF

Fig. 4 shows the polarization comparison plots of single cell and 5-cell stack with and without PFF. Fig. 4 (a) shows that the performance of VRFB single cell with and without PFF is almost similar. Both the cells show nearly 1.26 V at 100 mA cm^{-2} current density. But the five-cell stack (Fig. 4(b)) shows significant improvement in the galvanostatic polarization curve while having PFF. At 100 mA cm^{-2} about 5.3 V (1.06 V per cell) was realized with a stack devoid of PFF, whereas 6.25 V (1.25 V per cell) was obtained while having PFF. Around 200 mV per cell was the gain while using PFF. This improvement in cell voltage is attributed to the uniform distribution of the electric current density among all cells, as shunt current is minimized while using PFF.



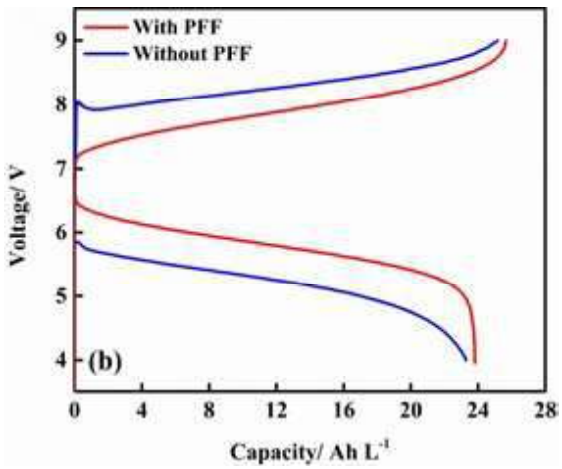


Fig. 5 (a) GCD performance comparison of 150 cm2 single cell and (b) 5 cells stack with and without PFF at 100 mA cm-2 current density using 1.6M vanadium electrolyte with 0.05M H3PO4 additive.

Fig. 5 (a) and (b) shows the 2nd cycle GCD profile comparison of 150 cm2 single cell and five cell stacks at 100 mA cm2 current density, respectively, using 1.6 M vanadium electrolyte (250 ml for each cell). The GCD profile of single cells was almost similar with and without PFF, whereas a significant improvement was observed in the five cells stack performance. Around 1 V improvement in the discharge voltage was observed at 12 Ah L-1 specific capacity. Also, the voltage efficiency of the stack was increased by 10 % from 62 % to 72 % with PPF compared to without PFF. GCD comparison plots indicate that the PFF could help suppress the shunt current losses, leading to the uniform distribution of the current in each stack cell, which improves the cell performance significantly.

3.2 Single-cell performance with and without H_3PO_4 additive in the electrolyte:

The Galvanostatic charge-discharge (GCD) performance of the VRFB single cell (Fig. 5(a)) using 1 litre of 1.6 M vanadium solution with and without 0.05M phosphoric acid additive is shown in Fig. 5(b). The discharge capacity of VRFB cells employing 1.6 M vanadium electrolyte with 0.05M of H_3PO_4 was around 25.8 Ah $L^{-1,}$ whereas it was only 23.4 Ah L^{-1} in the absence of H_3PO_4.

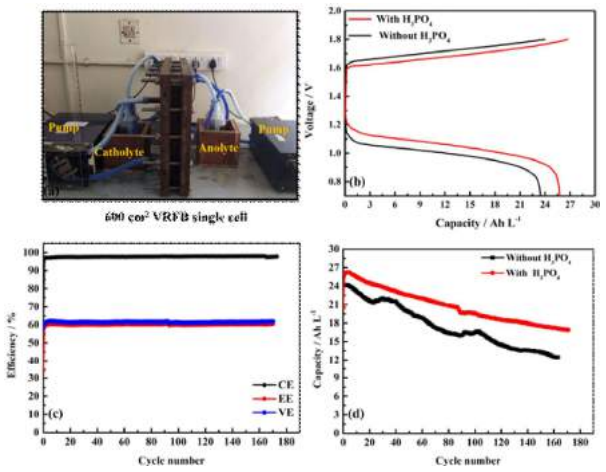


Fig. 6 (a) VRFB Single cell test set up (b) GCD performance comparison of single cell with and without H_3PO_4 additive (c) efficiencies of a single cell at 100 mA cm^{-2} current density using 1.6M vanadium electrolyte with 0.05M H_3PO_4 additive (d) capacity retention comparison plot.

According to Fig. 6 (b), the discharge capacity is higher by 2.4 Ah L^{-1} while having H_3PO_4 additive indicating a reduction in the over-potential of the charge-discharge process, leading to more electrolyte utilization within the voltage cut-off window. To understand the cycling stability of the modified electrolyte, the GCD was conducted at 100 mA cm^{-2} current density, as shown in Fig. 6(c & d). CE of VRFB cells with and without additive was almost identical (~98 %), but the VE has increased by 3 % with additive and consequently, EE jumps from 57 to 61 %, as shown in Fig. 6 (c). The capacity retention of VRFB cell without additive was only 52 % after 160 GCD cycles, whereas it was around 67 % in the presence of H_3PO_4 additive, as shown in Fig. 6 (d). Fabio *et al.* investigated the fundamental interactions of vanadium ions in all oxidation states in a mixed H_3PO_4-H_2SO_4 acid solution by DFT (density functional theory) and determined the possible solution structures of the vanadium cations in this electrolyte[30]. They have found that a small amount of the H_3PO_4 can reduce the charge transfer resistance, especially for the V^{3+}/V^{2+} redox couple by altering its solution structure (i.e., speciation). H_3PO_4 significantly reduces the polarization resistance associated with the V^{3+} reduction reaction.

3.3. 1 kW/ 10 kWh VRFB assembly and its electrical performance:

A1kW/10 kWh VRFB stack consisting of 24 cells in series was assembled. Figure 7 depicts the front view of the 1kW/10 kWh VRFB stack. To achieve 10 kWh of energy, 720 liters of 1.6 M vanadium solution with 0.05 M H_3PO_4 additive was used on both sides. The electrolytes were circulated using two magnetic pumps with a flow rate of around 15 lpm. Fig. 8 shows the galvanostatic polarization curve of (a) single cell and (b) 24-cell stack while using 1.6 M vanadium electrolyte with additive. The flow rate in the single-cell and stack were 0.6 lpm and 15 lpm, respectively. The cell voltage of a VRFB single cell is nearly 1.19 V, whereas the 24-cell stack is around 27.6 V (~1.15 V per cell) at 100 mA cm^{-2} current density. The stack can deliver a peak power of 1.44 kW when it is at 100 % state of charge.

The polarization study reveals that the voltage per cell of the stack is almost comparable to the single-cell voltage, which indicates reasonable control over the shunt current loss in the system developed.



Fig. 7. Front view of 1 kW/10 kWh VRFB stack with the piping arrangement

The charge-discharge performance of a 1 kW/ 10 kWh VRFB system (20 A charging and 1kW constant load discharge) using 720 L of 1.6 M vanadium electrolyte each side is shown in the Fig. 9. The stack delivers a capacity of 925 Ah at a nominal voltage of 30 V with 88 % CE.

Further, the stack was subjected to 300 shallow cycles (constant Ah charge-discharge) to understand the cycling stability. The stack was charged for one h at 20 A current and discharged at 60 A for 20 minutes. The end of stack voltage after each discharge was plotted against the cycle number (inset of Fig.

9). The stack realized a 79 % power retention after 300 shallow cycles.

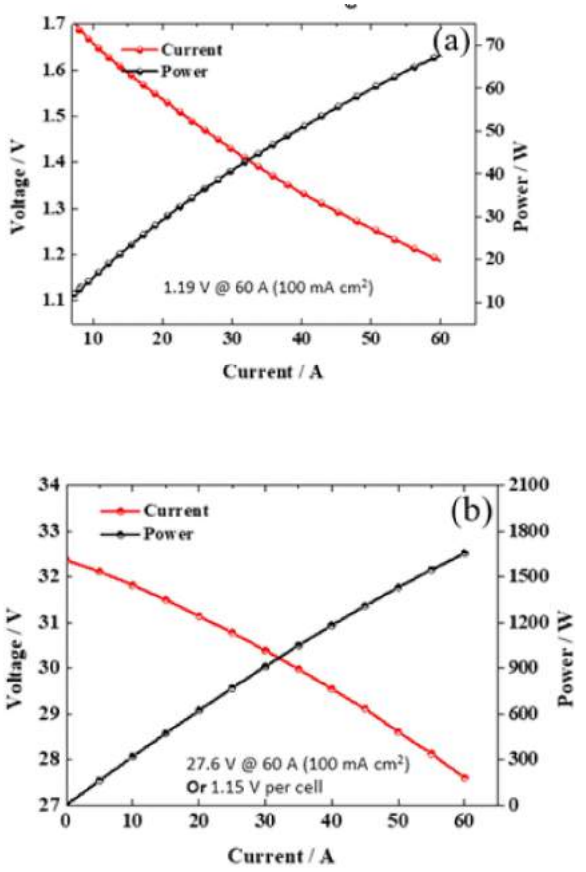


Fig. 8. Galvanostatic polarization (I-V) curve data of (a) single-cell and (b) 24-cell stack

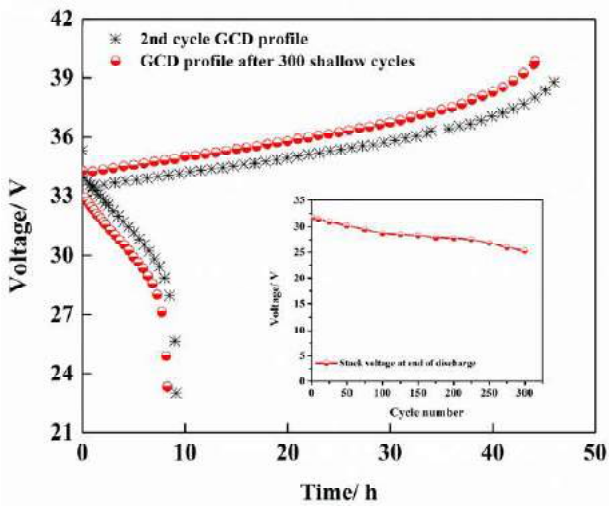


Fig. 9. GCD(cycling) data of 24- cells1kw/10kwh VRFB stack changed at 20A consent current whereas discharge at1KW constant load and end of discharge voltage VS cycle number plot of 300 shallow cycles performed at constant Ah(inset)

For the demonstration of the 1 kW/10 kWh VRFB stack with solar charging, the stack was coupled with six numbers of 400 W solar panels. The stack was charged up to 40 V at a constant current density of 33 mA cm^{-2} using solar power harvested during the day, and discharge was carried out using a 1 kW load (lights), as shown in Fig. 8. The VRFB stack delivered 1kW for 11 h continuously.



Fig. 10. Discharge of 1 kW/10 kWh VRFB stack with 1kW load

Conclusions

VRFB stack with a 1kW/10kWh power rating and new flow frame design was developed indigenously and demonstrated with solar PV charging. The 24 cells stack was built using two monopolar plates and 23 bipolar plates of 600 cm^2 active area to achieve a total power of 1.4 kW and energy of 10kWh VRFB ESS. After discounting energy for pumps/ inverter, the usable electricity was about 1 kW. The single cell and short 5 cells stack studies revealed the effect of non-conducting polymeric flow frame design in minimizing the shunt current losses at a common manifold. H_3PO_4 as an electrolyte additive was explored with the larger-sized electrode area and around 67 % of discharge capacity retention was observed, which is 15 % higher than the electrolyte without additive after 160 cycles at 100 mA cm^{-2} current density. In comparison to having an entire flow field plate out of graphite, the developed design gives a longer path for the vanadium solution to reach the electrically conducting portion of the flow plate and the flow plate is in touch with either anolyte or catholyte not to the both at the same time, thereby mitigates the shunt current. However, studies in different conditions, such as high altitudes and higher temperatures, need to be explored in the near future. Also, design optimization to reduce the weight, cost reduction and improvement in energy efficiency is to be considered for developing a self-sustaining energy storage system.

Acknowledgements

All the authors acknowledge the ONGC -Energy Centre Trust for financial support. Author HK acknowledges UGC for fellowship and the Indian Institute of Technology Madras (IITM) for facilities, MR acknowledges the IITM for the iPDF grant (No. CY21IPDF01).

References

1. K. Aydin and R. Kenanoðlu, *Int. J. Hydrogen Energy*, **43**, 14047–14058 (2018).
2. C. Di Bari,A. Lecocq, G. Marlair, B.Truchot, M. Mazzaro, M. L. Mele, P. Russo(2020, December). Recent safety focused overall analysis, testing and accident reviews towards safer e-mobility and energy storage. In International Conference on Fires In Vehicles (FIVE 2020).
3. H. L. Ferreira, R. Garde, G. Fulli, W. Kling, and J. P. Lopes, *Energy*, **53**, 288–298 (2013).
4. L. Zhang, R. Feng, W. Wang, and G. Yu, *Nat. Rev. Chem.* (2022).
5. Y. Yao, J. Lei, Y. Shi, F. Ai, and Y. C. Lu, *Nat. Energy 2021 66*, **6**, 582–588 (2021)
6. M. M. Rahman, A. O. Oni, E. Gemechu, and A. Kumar, *Environ. Assess. Renew. Energy Convers. Technol.*, 249–276 (2022).
7. A. A. Kebede, T. Kalogiannis, J. Van Mierlo, and M. Berecibar, *Renew. Sustain. Energy Rev.*, **159**, 112213 (2022).
8. P. Alotto, M. Guarnieri, and F. Moro, *Renew. Sustain. Energy Rev.*, **29**, 325–335 (2014).
9. T. Shigematsu, T. Kumamoto, H. Deguchi, and T. Hara, *Proc. IEEE Power Eng. Soc. Transm. Distrib. Conf.*, **2**, 1065–1070 (2002).
10. A. Z. Weber M. M. Mench, J. P. Meyers, P. N. Ross, J. T. Gostick and Q. Liu *J. Appl. Electrochem.*, **41**, 1137–1164 (2011).
11. T. Davies and J. Tummino, *Journal of carbon research*, **4**, 8 (2018).
12. B. Turker, S. Arroyo Klein, E. M. Hammer, B. Lenz, and L. Komsiyska, *Energy Convers. Manag.*, **66**, 26–32 (2013).
13.
14. L. Barelli, G. Bidini, P. A. Ottaviano, and D. Pelosi, *J. Energy Storage*, **24**, 100770 (2019).
15. K. L. Huang, X. gang Li, S. qin Liu, N. Tan, and L. quan Chen, *Renew. Energy*, **33**, 186–192 (2008).
16. H. Khan, R. Murugan, and K. Ramanujam, *J. Electrochem. Soc.*, **168**, 100542–100552 (2021)
17. M. Raja, H. Khan, S. Sankarasubramanian, D. Sonawat, and V. Ramani, *Catal. Today*, **15**,
18S. Kim SKim, E. Thomsen. G. Xi, Z. NieJ. Bao, K. Recknagle, W. Wang, V. Viswanathan, Q. Luo, X. Wei, A. Crawford, G. Coffey, G. Maupin and V. Sprenkle*J. Power Sources*, **237**, 300–309 (2013).
19. R. Gundlapalli, S. Kumar, and S. Jayanti, *Ina. Lett. 2018 33*, **3**, 149–157 (2018)
20. A. Trovò, F. Picano, and M. Guarnieri, *J. Power Sources*, **440**, 227144 (2019).
21. F. Xing, H. Zhang, and X. Ma, *J. Power Sources*, **196**, 10753–10757 (2011).
22. D. J. Park, K. S. Jeon, C. H. Ryu, and G. J. Hwang, *J. Ind. Eng. Chem.*, **45**, 387–390 (2017).
23. Y. Huang, J. Huo, S. Dou, K. Hu, and S. Wang, *RSC Adv.*, **6**, 66368–66372 (2016)
24. A. Parasuraman, T. M. Lim, C. Menictas, and M. Skyllas-Kazacos, *Electrochim. Acta*, **101**, 27–40 (2013).
25. A. W. Bayeh, D. M. Kabtamu, Y. Chang, T. H. Wondimu, H-CHuang and C-H Wang, *Sustain. Energy Fuels*, **5**, 1668–1707 (2021)
26. R. Zhang, X. Jing, Y. Chu, L Wang, W. Kang, D. Wei, H. Li and S. Xiong, *J. Mater. Chem. A*, **6**, 17730–17739 (2018)
27. Z. Li, J. X. H. Zhou, L. Liu, Z. Wu, X. Qiu and L. Chen, *J. Power Sources*, **237**, 132–140 (2013).
28. D. Reed , E. Thomsen, W. Wang, Z. Nie, B.Li, X. Wei, B. Koeppel, VSprenkle, *J. Power Sources*, **285**, 425–430 (2015).
29. V. Mahanta, R. M., H. Khan, and K. R., *J. Electrochem. Soc.*, **167**, 160504 (2020).
30. F. J. Oldenburg, M. Bon, D. Perego, D. Polino, T. Laino, L. Gubler and T. J. Schmidt,*Phys. Chem. Chem. Phys.*, **20**, 23664–23673 (2018)